Field measurement of upper ocean turbulence dissipation associated with wave-turbulence interaction in the South China Sea

Chuan Jiang Huang,[1] Fangli Qiao,[1] Dejun Dai,[1] Hongyu Ma,[1] and Jingsong Guo[1]

Received 4 December 2011; revised 22 March 2012; accepted 29 March 2012; published 12 May 2012.

[1] The turbulence dissipation rate within the mixed layer was measured in the open ocean and the coastal water of the South China Sea under moderate winds of 4.7 $\sim$ 8.9 m s^{-1} using a free-falling MSS profiler. In the open ocean, the profile of the dissipation rate within the mixed layer exhibited an exponential decay with the depth at most stations, which was satisfactorily consistent with that predicted by the parameterization of wave-turbulence interaction presented by Huang and Qiao (2010) while deviating from that by the law of the wall. In the coastal ocean, however, both the parameterization of wave-turbulence interaction and the law of the wall can give approximate predictions to the measured dissipation rate.

Citation: Huang, C. J., F. Qiao, D. Dai, H. Ma, and J. Guo (2012), Field measurement of upper ocean turbulence dissipation associated with wave-turbulence interaction in the South China Sea, *J. Geophys. Res.*, *117*, C00J09, doi:10.1029/2011JC007806.

1. Introduction

[2] The turbulence plays an important role in the heat, momentum, and energy balances of the ocean. The upper mixed layer is one of regions with strong turbulence in the ocean. It is believed that surface waves at the air-sea interface exert a dominating influence on the budget of turbulence kinetic energy (TKE) for the mixed layer. The surface waves can affect the turbulence in a variety of ways, such as wave breaking and wave-turbulence interaction. Most of wave energy is locally dissipated through wave breaking [*Donelan*, 1998], which greatly enhances the TKE near sea surface [*Agrawal et al.*, 1992; *Drennan et al.*, 1996]. However, the strong turbulence induced by wave breaking is mainly confined within the near-surface zone with the depth scale of wave height [*Rapp and Melville*, 1990; *Craig and Banner*, 1994]; at greater depths, its effect is very limited [*Soloviev and Lukas*, 2003; *Huang et al.*, 2011].

[3] Wave-turbulence interaction can directly transfer energy from the surface waves to the turbulence because the surface waves are not truly irrotational or potential before breaking. Over past decades, wave-turbulence interaction has been confirmed by theoretical analyses, laboratory experiments, and field observations. *Phillips* [1961] argued that the viscosity effect in the ocean can get energy from surface waves. Laboratory experiments by *Cheung and Street* [1988] indicated that interactions among the mean current, waves and turbulence fields always occur in the wind-ruffled mechanically generated wave cases, in which the energy transfer from the wavefield to the mean current by the wave-induced Reynolds stress, and in turn transfer to turbulence by the turbulence viscosity. *Thais and Magnaudet* [1996] also pointed out that the structure of the turbulent field below surface waves was different from that near a wall. Subsequently, these results were confirmed by field experiments [*Anis and Moum*, 1995], which showed similar wave-turbulence interaction in the real ocean when the swells were present. *Qiao et al.* [2004] analytically expressed the nonbreaking wave-induced vertical mixing as the function of wave number spectrum, and the surface wave-induced mixing which can be exactly calculated from a wave numerical model much improves the performances of different circulation models [*Qiao et al.*, 2010; *Wang et al.*, 2010; *Shu et al.*, 2011] and climate models [*Huang et al.*, 2008; *Song et al.*, 2011]. Based on dissipation measurements from a surface-following float in the open ocean, *Gemmrich and Farmer* [2004] analyzed the turbulence structure beneath breaking and nonbreaking waves, and found that the occurrence and magnitude of the prebreaking turbulence were consistent with that induced by wave-turbulence interaction in a rotational wavefield. Recently, field observation by *Veron et al.* [2009] and laboratory experiments by *Babanin and Haus* [2009] and *Dai et al.* [2010] further revealed the existence of turbulence induced by wave-turbulence interaction.

[4] Compared with wave breaking, the TKE associated with wave-turbulence interaction can affect a greater depth, and plays an important role in regulating the vertical mixing and thermal structure of the upper ocean. Recently, *Huang and Qiao* [2010] presented a parameterization of the TKE dissipation rate induced by wave-turbulence interaction as

$$\varepsilon_{wave} = 148\beta\sqrt{\delta}\frac{u_{s0}u_*^2}{L}e^{2kz}, \quad (1)$$

where β is a dimensionless constant. δ (=H_s /L) is the wave steepness, H_s is the significant wave height, and L is the

[1]Key Laboratory of Marine Science and Numerical Modeling, First Institute of Oceanography, State Oceanic Administration, Qingdao, China.

Corresponding author: F. Qiao, Key Laboratory of Marine Science and Numerical Modeling, First Institute of Oceanography, State Oceanic Administration, 6 Xianxialing Rd., Qingdao 266061, China. (qiaofl@fio.org.cn)

0148-0227/12/2011JC007806

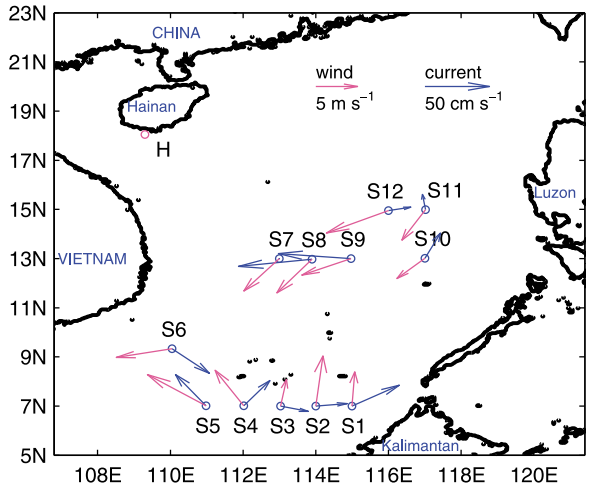

Figure 1. Location of the stations in the South China Sea, with surface wind velocities (pink arrows) and current velocities (blue arrows) during the measurement.

wavelength, $u_{s0} = c(Ak)^2$ is the magnitude of the Stokes drift at the surface ($z = 0$), here c is the wave phase velocity, A ($=H_s/2$) is the wave amplitude, and k ($=2\pi/L$) is the wave number, $u* = \sqrt{\tau/\rho_w}$ is the friction velocity in the water, here τ is the surface wind stress, and ρ_w is the water density, and z is the vertical coordinate with zero at the mean sea level and positive upward. In this parameterization, the TKE dissipation rate induced by wave-turbulence interaction is a function of $u_{s0}u_*^2$ and wave parameters, and it decays with the depth away from the surface in the form of e^{2kz}. This scheme has been incorporated into the Mellor-Yamada scheme as an additional source of turbulence [*Huang et al.*, 2011]. The results showed that wave-turbulence interaction can effectively amend the problem of insufficient upper ocean mixing in the classic Mellor-Yamada scheme, then the simulated turbulence characteristics and upper ocean thermal structure were significantly improved compared to the original model.

[5] In this study we compared the measured dissipation rate in the South China Sea (SCS) with that predicted by this parameterization scheme of wave-turbulence interaction, as well as that by the law of the wall. The detail of the measurement was described in section 2. The measured dissipation rate and those predicted by wave-turbulence interaction and the law of the wall were given in section 3. A brief conclusion was presented in section 4.

2. Measurements and Methods

[6] Microstructure turbulence measurements were performed in the deep ocean from 29 October to 10 November 2010 and coastal ocean on 14 November 2010. The 21 turbulence stations located in the central south part of SCS with a water depth ranging from 1427 to 4372 m, in which the 9 stations were discarded due to instrument malfunction. The data from the other 12 stations, named as S1 ~ S12, were used to examine the effect of wave-turbulence interaction on the upper ocean in this study (Figure 1). A survey overview was given in Table 1.

[7] Vertical profiles of turbulence dissipation rate ε were made with a 1.0 m long loosely tethered free-falling MSS profiler. The MSS profiler is an instrument for measuring small-scale turbulence and hydrographic parameters, which is equipped with high-resolution microstructure sensors measuring the small-scale velocity shear and temperature fluctuations, standard conductivity-temperature-depth (CTD) sensors, and house-keeping sensors measuring profiler accelerations [*Prandke and Stips*, 1998]. All sensors sample at 1024 Hz to 16 bit resolution.

[8] In these measurements, the sinking operation of the MSS profiler was used with a typical sinking velocity of 0.75 m s^{-1}. At these 12 stations, three casts of the profiler were performed except for Stations S3 and S10. At these two stations, only two casts were performed because the loosened cable tethered the profiler was very close to and rubbed sometimes with the vessel hull during measuring.

[9] The CTD casts were combined to provide measurements of temperature and salinity. A lowered acoustic Doppler current profile (LADCP) mounted on the CTD frame was used to measure the mean current. Wind velocities were measured by a ship-mounted automatic measuring system at 19.5 m height above the water surface, and adjusted to the standard height of 10 m assuming the neutral stability. The wind stress τ was calculated from the bulk formula as

$$\tau = \rho_a c_d u_{10}^2, \tag{2}$$

Table 1. The Location, Water Depth, Time, Wind Speed at 10 m Height During the Measurement at Stations S1 ~ S12; Significant Wave Height H_s and Period T_s From the ERA-Interim Reanalysis; and the Dimensionless Constant β in Equation (1)[a]

Station	Position (Latitude, Longitude)	Depth (m)	Time (UTC)	Wind (m s^{-1})	H_s (m)	T_s (s)	β
S1	7°00′N, 115°00′E	2909	29 Oct, 04:08 ~ 04:33	6.0	2.1	9.7	0.25
S2	7°00′N, 114°00′E	2073	29 Oct, 11:46 ~ 12:16	8.9	1.9	10.0	0.20
S3	7°00′N, 113°02′E	1427	29 Oct, 18:52 ~ 19:15	4.7	2.0	9.9	0.45
S4	7°01′N, 112°01′E	2035	30 Oct, 04:37 ~ 04:58	7.1	2.0	9.8	0.20
S5	7°01′N, 110°59E	1765	30 Oct, 11:53 ~ 12:14	8.9	2.2	10.6	1.0
S6	9°20′N, 110°03′E	2335	1 Nov, 02:11 ~ 02:31	6.8	2.7	10.6	0.25
S7	13°00′N, 113°00′E	4078	6 Dec, 12:40 ~ 13:00	7.1	2.1	10.0	0.6
S8	12°58′N, 113°54′E	4276	6 Dec, 22:39 ~ 23:13	7.3	1.9	9.6	1.5
S9	13°00′N, 114°58′E	4372	7 Dec, 08:44 ~ 09:16	6.5	1.6	8.9	0.5
S10	13°01′N, 117°00′E	4121	8 Dec, 04:07 ~ 04:22	4.9	1.3	8.2	1.5
S11	14°59′N, 117°01′E	4268	9 Dec, 02:02 ~ 02:23	6.1	1.9	8.4	1.0
S12	14°57′N, 116°00′E	4277	10 Nov, 10:09 ~ 10:31	8.4	2.5	10.7	1.0

[a]The significant wave period T_s was calculated by a linear formula $T_s = 1.125T_m$ [*Wen and Yu*, 1984], where T_m was the mean wave period.

Table 2. The Time, Wind Speed at 10 m Height, and Significant Wave Height H_s and Period T_s During the Measurement at Station H[a]

	Time (UTC)				
	03:00	04:00	05:00	06:00	07:00
Wind (m s^{-1})	4.9	5.9	6.1	6.1	6.2
H_s (m)	2.0	2.0	1.8	1.9	1.8
T_s (s)	7.0	7.1	7.5	7.0	7.1

[a]The wave parameters were measured by the Datawell Waverider directional wave buoy. The constant β in equation (1) was set to 1.0 because instrument-measured wave parameters were used.

where ρ_a was the air density, u_{10} was the wind speed at 10 m, and c_d was the drag coefficient with a value of 1.2×10^{-3} for the winds between 4 and 11 m s^{-1} [*Large and Pond*, 1981].

[10] An additional station, named as H located on the south of the Hainan Island with a water depth of 50 m, in which three casts of the profiler were performed every hour (Table 2). The measurement was sustained about 5 h, and then stopped due to the activity of fishing boats.

[11] Shear raw data measured by the MSS profiler can be polluted by anomalous spikes resulting from plankton particles, and low- and intermediate-frequency disturbances from profiler vibrations and the brushes at the aft end of the profiler [*Wolk et al.*, 2002]. In order to remove spikes, the raw shear data were first checked by the local standard deviation (for data segments of 40 measured points) and filtered by the Butterworth low pass with a cutoff frequency of 80 Hz [*Stips and Prandke*, 2000]. The TKE dissipation rate ε was calculated using the equation for isotropic turbulence

$$\varepsilon = 7.5\nu\overline{(\partial u'/\partial z)^2}, \tag{3}$$

where $\partial u'/\partial z$ is the vertical profile of the horizontal velocity shear, and ν is the viscosity which is a function of the local water temperature. The velocity shear variance $\overline{(\partial u'/\partial z)^2}$ was calculated by integrating the power spectrum for data segments of 2048 measured points (corresponding to depth segments of 1.5 m for a sinking velocity of 0.75 m s^{-1}) over a wave number range from 2 cpm to k_c, where $k_c = (\varepsilon/\nu^3)^{1/4}/2\pi$ is the Kolmogorov wave number. Because the k_c is a function of the ε, an iterative procedure was used to calculate the shear variance, and thus the ε.

[12] The Nasmyth's universal spectrum is an empirical spectrum of oceanic turbulence proposed by *Nasmyth* [1970], whose analytical form is as follows:

$$\Psi_N = 8.05\frac{(k/k_c)^{1/3}}{1+(20\times k/k_c)^{3.7}}, \tag{4}$$

where k is the wave number. The measured oceanic turbulence spectra are routinely compared to the empirical turbulence spectrum.

[13] In this study, some data deviated greatly from the universal spectrum were discarded. The ideal systematic bias of the ε measured by the MSS profiler is estimated to be within the factor of 2. However, there may have a larger uncertainty in routine measurements. The detailed algorithm and description for calculating the ε can refer to *Stips and Prandke* [2000] and *Stips* [2005].

[14] Figure 2 showed the shear spectra at specified depth segments for the first cast at 06:00 UTC at Station H, which were approximately consistent with the Nasmyth's universal spectrum, although they still had some spikes. At these segments, the ε obtained from the measured spectra ranged from about $2 \times 10^{-9} \sim 8 \times 10^{-8}$ m^2 s^{-3}.

[15] Wave parameters were collected with a Datawell Waverider directional wave buoy (DWR) at Station H. However, instrument-measured wave parameters were not available at Stations S1 ~ S12. Instead, the outputs from the ERA-Interim reanalysis [*Dee et al.*, 2011] were used to predict the ε induced by wave-turbulence interaction (Table 1). The significant wave period was calculated by a linear formula $T_s = 1.125T_m$ [*Wen and Yu*, 1984], where T_m was the mean wave period. The data had a horizontal resolution of 0.75° × 0.75° and a time resolution of 6 h, and was linearly interpolated to the measured location and time.

3. Results

3.1. Measurements in the Open Ocean

[16] The SCS is a large quasi-enclosed marginal sea in the western Pacific with a maximum depth over 5000 m (Figure 1). The SCS is controlled by the Southeast Asia monsoon system, which is dominated by the southwesterly

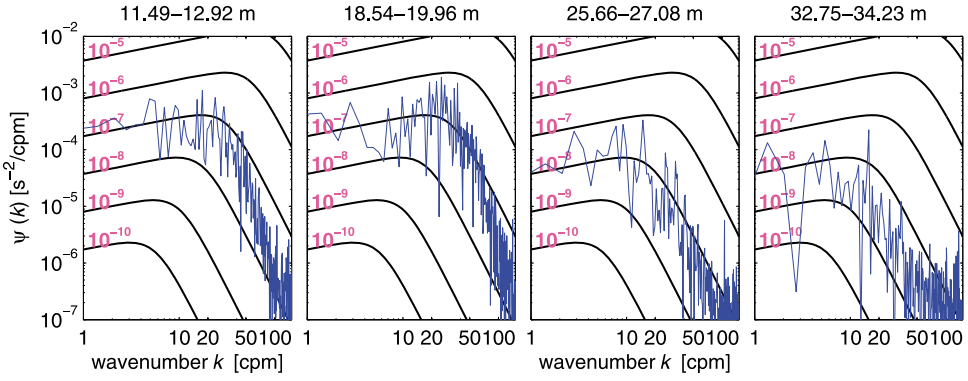

Figure 2. Examples of the dissipation spectrum of the velocity shear at specified depth segments for the first cast at 06:00 UTC at Station H. The smooth curves were the Nasmyth universal spectra for various dissipation rates.

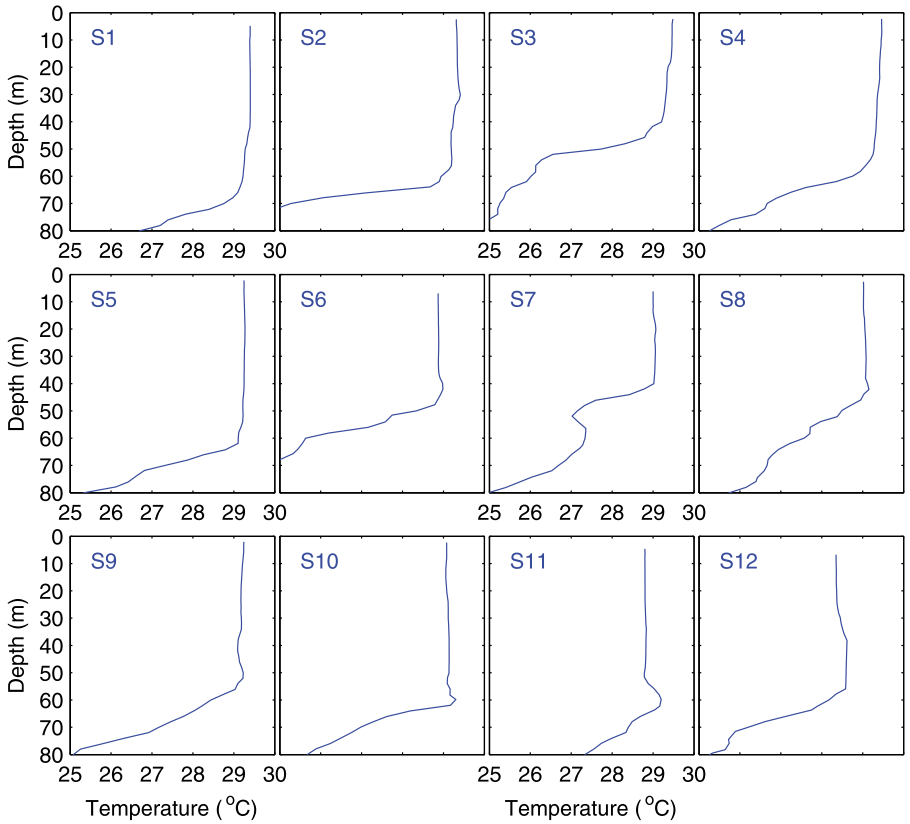

Figure 3. Vertical profiles of temperature measured by the CTD at Stations S1 ∼ S12 (in °C, the data resolution was 2 m).

winds in summer, but northeasterly winds in winter. The circulation of the SCS is mostly affected by the monsoon winds due to the absence of major oceanic inflow [*Wyrtki*, 1961].

[17] The measurements at Stations S1 ∼ S12 were conducted from 29 October to 10 November 2010, which was in the seasonal transition period from the summer monsoon to the winter monsoon. The measured sites were dominated by the south or southeast winds with speeds from 4.7 to 8.9 m s^{-1} at the first 5 stations (S1 ∼ S5), while by the northeast winds at subsequent stations (Figure 1).

[18] At these 12 stations, the mixed layers were about 40 ∼ 60 m with a temperature of about 29°C (Figure 3). Beneath the mixed layer, there was a pronounced thermocline. The currents of the upper ocean varied from 17.7 (at Station S11) to 57.6 cm s^{-1} (at Station S8). The current velocities were almost identical within the upper 50 m (Figure 4), which flowed eastward or northeastward at the Stations S1 ∼ S4, but westward in Stations S8 ∼ S9 (Figure 1). The current suggests an anticlockwise gyre in the region, which was frequently reported by previous studies [*Fang et al.*, 2002; *Hwang and Chen*, 2000].

[19] Figure 5 showed the measured dissipation rate (named as ε_m) at these 12 stations. The ε_m in the upper 10 m was discarded because of contaminations by the vessel's wake, as well as influences of wave breaking. The ε_m showed somewhat scatter at some stations, which may be related to the high intermittency of turbulence in time and space [*Shay and Gregg*, 1986; *Soloviev and Lukas*, 2003]. The magnitude of the ε_m was large on the order of $10^{-7} \sim 10^{-6}$ m^2 s^{-3} at 10 m depth, and decreased rapidly to the order of 10^{-9} m^2 s^{-3} in the lower mixed layer. At most of stations, the ε_m showed an exponential decay with the depth, which was similar to observations by *Anis and Moum* [1995] and *Wüest et al.* [2000].

[20] The ε_m was compared with that predicted by wave-turbulence interaction using equation (1), which was named as ε_{wave}. The significant wave height H_s and period T_s were needed for calculating ε_{wave} in this equation. Wave parameters from the ERA-Interim reanalysis were used at these stations since no instrument-measured wave parameters. The magnitude of ε_{wave} was highly sensitive to the values of H_s and T_s. A constant β was used for fitting the ε_{wave} to ε_m, which can partly offset the uncertainty induced by reanalyzed wave parameters (Table 1).

[21] It can be seen that the ε_m was in good agreement with the ε_{wave} at most stations. Figure 6 showed the correlation coefficient R of the common logarithm of the ε_m with that of the ε_{wave} at these stations, in which the R was defined as

$$R = \sqrt{1 - \sum (Y - Y_2)^2 / (Y - Y_1)^2}, \tag{5}$$

where $Y = \log_{10}\varepsilon_m$, Y_1 was its mean, and $Y_2 = \log_{10}\varepsilon_{wave}$. The R was all statistically significant at the 95% confidence level, which can reach to 0.75 ∼ 0.86 at most of stations. The value of the R was only 0.37 at Station S8. At this station, the ε_m was almost identical between 10 and 40 m depth, as opposed to decaying exponentially with depth. Therefore, the parameterization of wave-turbulence interaction failed to make a good prediction for the ε_m.

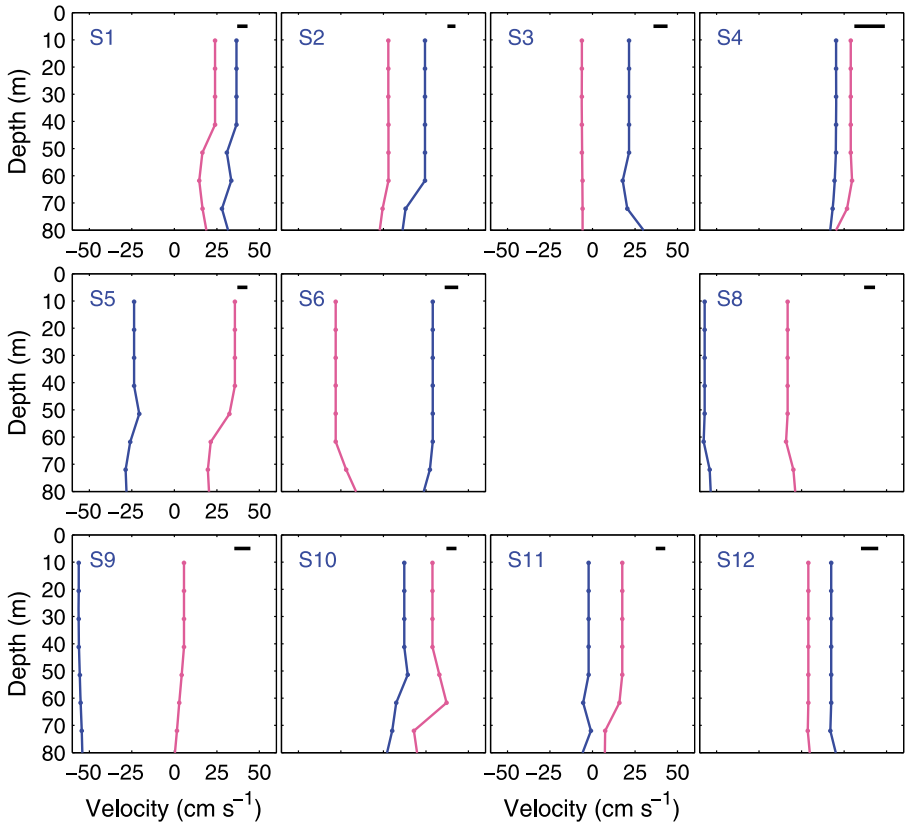

Figure 4. Vertical profiles of the zonal velocity (blue lines) and meridional velocity (pink lines) measured by the LADCP at Stations S1 ∼ S12 (in cm s^{-1}, the data resolution was 10 m). The black line was the maximum calculation errors of the velocity. The data at Station S7 was not available due to poor data quality.

[22] At Stations S3 and S9, the values of the R were about 0.59, which were largely associated with relative small ε_m in the middle of the mixed layer. At Station S1, the ε_m presented a zigzag profile, which was much smaller at 20 ∼ 30 m depth, while larger at 30 ∼ 40 m compared with the ε_{wave}. The reason remains unclear, but the problem of the instrument can be eliminated because the profiles from three casts exhibited a similar structure. At Station S10, relative large ε_m was also measured under 40 m depth, which may be caused by the shear of the mean current (Figure 4).

[23] Some studies predicted the ε_m of the upper ocean with the law of the wall [*Osborn et al.*, 1992; *Ozen et al.*, 2006], which was represented by

$$\varepsilon_{wall} = u_*^3/\kappa z, \tag{6}$$

where κ = 0.41 was the von Karman constant. The ε_{wall} made a good prediction to the ε_m of the upper 40 m at Station S8, and approximate predictions at Stations S5, S11, and S12, while failed to predict their ε_m under 40 m depth (Figure 5). At the other stations, it seemed that the ε_{wall} failed to predict the ε_m, where the ε_{wall} was greatly deviated from the ε_m throughout the mixed layer.

[24] From equation (6), it can be seen that the ε_{wall} was directly dependent on the surface wind speed (or the wind stress) because the friction velocity u_* was a function of the wind stress. Therefore, the ε_{wall} should be identical for the same wind speeds. However, for stations with almost the same winds, such as S2 and S5 with wind speeds of 8.9 m s^{-1}, the measured ε_m differed substantially although the ε_{wall} was almost identical (Figure 7). For other stations, such as S4 and S7, the ε_m also showed similar results. This may imply that the ε_m in the upper ocean was not dominated by the surface winds (or the law of the wall) at these stations, but other processes, such as wave-turbulence interaction.

3.2. Measurements in the Coastal Ocean

[25] The measurement at Station H was performed on 14 November 2010. The water depth was about 50 m at this station. The dissipation measurements were ended at 45 m depth, but only the data between 10 and 40 m depth were used for analysis in order to exclude effects of the vessel's wake and wave breaking in the surface and the cable tension in the bottom. This measurement was conducted only about 5 h, and then stopped due to the activity of fishing boats. The winds were about 8 m s^{-1} before the measurement, then decreasing to 4 ∼ 6 m s^{-1}. The significant wave height was about 1.8 ∼ 2.0 m, and period was 7.0 ∼ 7.5 s during the measurement (Table 2).

[26] The CTD cast was not made in this station, so the temperature measured by the MSS profiler was used, which was shown in Figure 8. The measurements at Stations S1 ∼ S12 showed the temperatures measured by the two instruments agreed satisfactorily in the mixed layers. At 03:00 UTC, the water was well mixed throughout the depth with a temperature of 26.54°C. Under the surface heat flux,

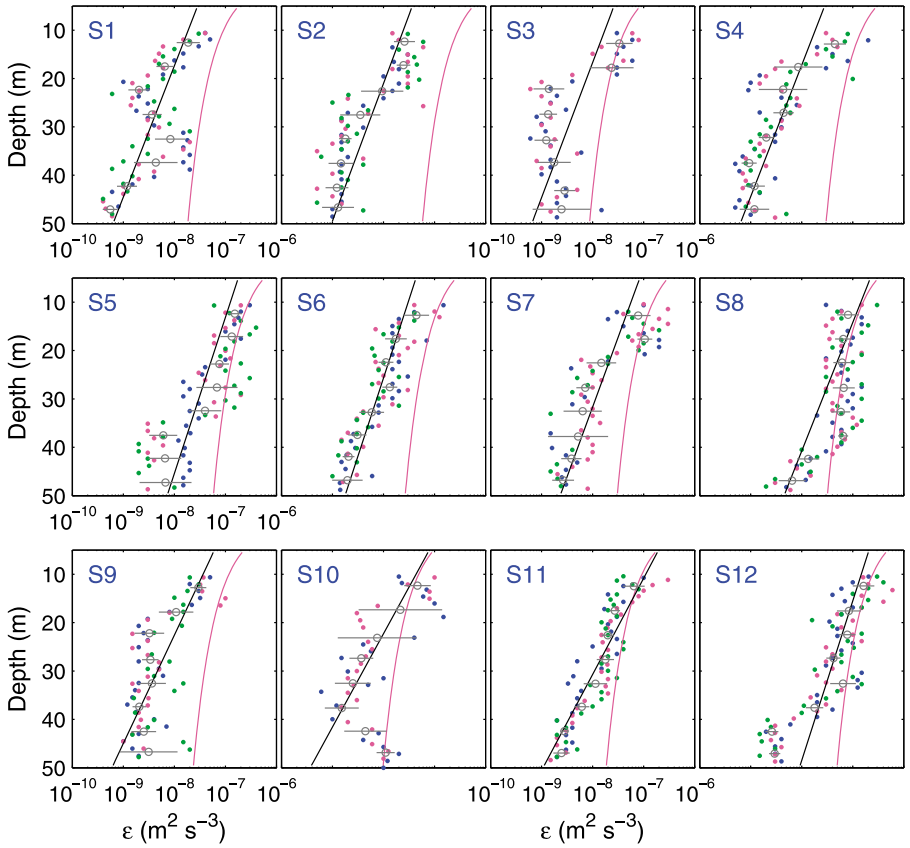

Figure 5. Vertical profiles of the measured dissipation rates ε_m (dots), and those predicted by wave-turbulence interaction ε_{wave} (black lines) and the law of the wall ε_{wall} (pink lines) at Station S1 $\sim$ S12 (in $m^2\ s^{-3}$). The blue, pink, and green dots represented the ε_m measured by the first, second, and third cast at each station, respectively. The gray circles were the mean of the common logarithm of the ε_m at 5 m depth intervals, and the gray lines were their 95% confidence intervals.

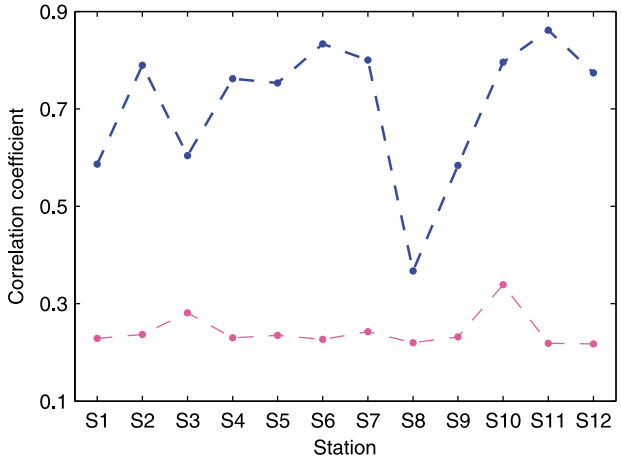

Figure 6. The correlation coefficient R of the common logarithm of the measured dissipation rates ε_m and those predicted by wave-turbulence interaction ε_{wave} (blue dots) at Station S1 $\sim$ S12. The pink dots were their 95% confidence threshold. The R was calculated from the ε_m between 10 and 40 m depth at Station S10, while it was calculated from the ε_m between 10 and 50 m depth at the other stations.

the water became warm, and a very weak mixed layer began to occur with a depth of 30 m. At 07:00 UTC, the temperature in the mixed layer increased about 0.09°C, and became to 26.63°C.

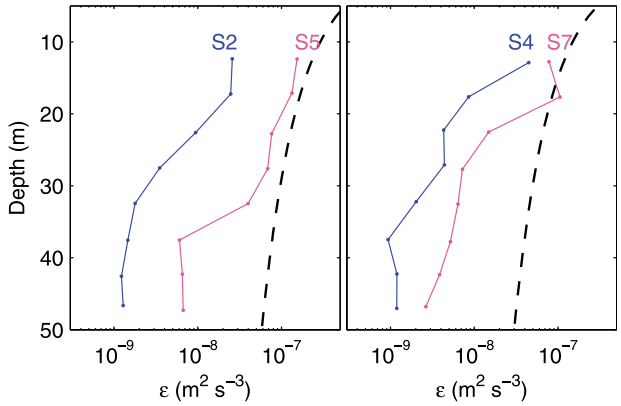

Figure 7. The mean of the common logarithm of the measured dissipation rates ε_m at 5 m depth intervals (left) at Stations S2 (blue line) and S5 (pink line) and (right) at Stations S4 (blue line) and S7 (pink line). The black dashed lines were the dissipation rates predicted by the law of the wall.

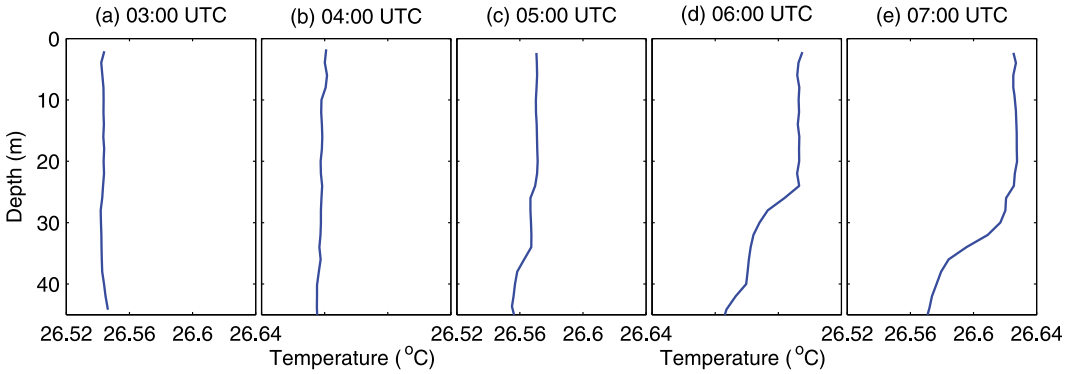

Figure 8. Vertical profiles of the temperature measured by the MSS profiler at Station H (in °C, the data resolution was 2 m).

[27] Figure 9 showed the measured dissipation rate ε_m and that predicted by wave-turbulence interaction ε_{wave}, as well as that by the law of the wall ε_{wall} at this station. The constant β in equation (1) was set to 1.0 because instrument-measured wave parameters were used. The water depth was only 50 m at this station. Besides of processes from the surface, the turbulence dissipation was largely influenced by those from the bottom boundary layer [*Wüest et al.*, 2000] and the tide [*Simpson et al.*, 1996]. Therefore, different from Stations S1 $\sim$ S12, both the ε_{wave} and ε_{wall} can give approximate predictions to the ε_m at this station.

4. Conclusions

[28] The turbulence dissipation rate within the mixed layer was measured in the SCS using a free-falling MSS profiler. In the open ocean, the profile of the measured dissipation rate within the mixed layer exhibited an exponential decay with the depth at most of stations, which was consistent with that predicted by wave-turbulence interaction, but deviated significantly from that by the law of the wall. At these stations, correlation coefficients of the common logarithm of the measured dissipation rate with that predicted by wave-turbulence interaction were all statistically significant at the 95% confidence level. In the coastal ocean, however, both wave-turbulence interaction and the law of the wall can give approximate predictions to the measured dissipation rate.

[29] The measured dissipation rate in the open ocean was expected to be correlated with effects of wave-turbulence interaction, because this analysis was restricted in the mixed layer between 10 and 50 m, where effects of wave breaking at the surface and internal waves in the thermocline play a minor role in the turbulence of this region. Due to the coarse current measurement and absence of the surface heat flux, further detailed study was limited.

[30] The parameterization scheme of wave-turbulence interaction obtained by *Huang and Qiao* [2010] was used to predict the measured dissipation rate in this study. This scheme was supported by these measurements. It gave satisfactory predictions for the measured dissipation rate at most of stations. However, the data were limited. Therefore, further measurements of the dissipation rate under various sea states, along with wave properties, the current and the surface heat flux, were necessary to robustly fix this scheme.

[31] **Acknowledgments.** The data are provided by the project "Responses of Marine Hazards to Climate Change in the Western Pacific (ROSE)" under framework of Intergovernmental Oceanographic Commission of UNESCO. The authors thank Zhixin Zhang for processing the LADCP data. This study was supported by the National Natural Science Foundation of China through grant 40806017 and 40876015, Public

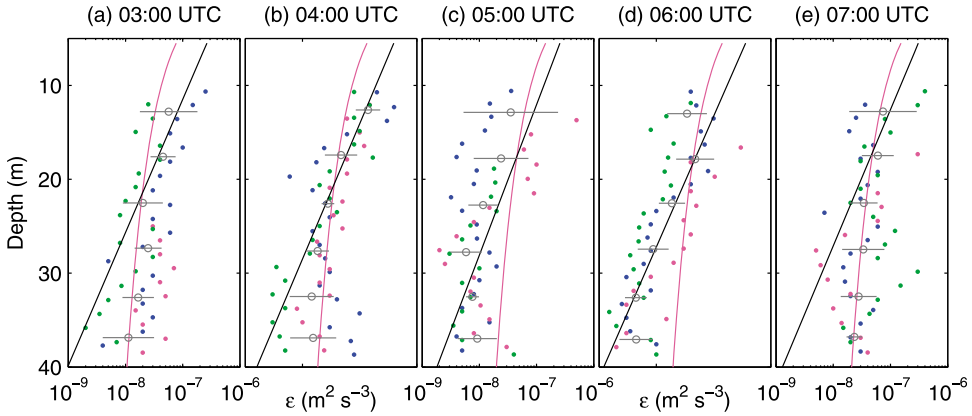

Figure 9. Same as Figure 5 but for Station H.

Science and Technology Research Funds projects of ocean (201105019), and international cooperation project of Ministry of Science and Technology of China (S2011GR0348).

References

Agrawal, Y. C., E. A. Terray, M. A. Donelan, P. A. Hwang, A. J. Williams III, W. M. Drennan, K. K. Kahma, and S. A. Kitaigorodskii (1992), Enhanced dissipation of kinetic energy beneath surface waves, *Nature*, *359*, 219–220, doi:10.1038/359219a0.

Anis, A., and J. N. Moum (1995), Surface wave-turbulence interactions: Scaling $\epsilon(z)$ near the sea surface, *J. Phys. Oceanogr.*, *25*, 2025–2045, doi:10.1175/1520-0485(1995)025<2025:SWISNT>2.0.CO;2.

Babanin, A. V., and B. K. Haus (2009), On the existence of water turbulence induced by nonbreaking surface waves, *J. Phys. Oceanogr.*, *39*, 2675–2679, doi:10.1175/2009JPO4202.1.

Cheung, T. K., and R. L. Street (1988), The turbulent layer in the water at an air-water interface, *J. Fluid Mech.*, *194*, 133–151, doi:10.1017/S0022112088002927.

Craig, P. D., and M. L. Banner (1994), Modeling wave-enhanced turbulence in the ocean surface layer, *J. Phys. Oceanogr.*, *24*, 2546–2559, doi:10.1175/1520-0485(1994)024<2546:MWETIT>2.0.CO;2.

Dai, D. J., F. Qiao, W. Sulisz, L. Han, and A. Babanin (2010), An experiment on the non-breaking surface-wave-induced vertical mixing, *J. Phys. Oceanogr.*, *40*, 2180–2188, doi:10.1175/2010JPO4378.1.

Dee, D. P., et al. (2011), The ERA-Interim reanalysis: Configuration and performance of the data assimilation system, *Q. J. R. Meteorol. Soc.*, *137*, 553–597, doi:10.1002/qj.828.

Donelan, M. A. (1998), Air-water exchange processes, in *Physical Processes in Lakes and Oceans*, *Coastal Estuarine Stud. Ser.*, vol. 54, edited by J. Imberger, pp. 19–36, AGU, Washington, D. C.

Drennan, W. M., M. A. Donelan, E. A. Terray, and K. B. Katsaros (1996), Oceanic turbulence dissipation measurements in SWADE, *J. Phys. Oceanogr.*, *26*, 808–815, doi:10.1175/1520-0485(1996)026<0808:OTDMIS>2.0.CO;2.

Fang, W., G. Fang, P. Shi, Q. Huang, and Q. Xie (2002), Seasonal structures of upper layer circulation in the southern South China Sea from in situ observations, *J. Geophys. Res.*, *107*(C11), 3202, doi:10.1029/2002JC001343.

Gemmrich, J. R., and D. M. Farmer (2004), Near-surface turbulence in the presence of breaking waves, *J. Phys. Oceanogr.*, *34*, 1067–1086, doi:10.1175/1520-0485(2004)034<1067:NTITPO>2.0.CO;2.

Huang, C. J., and F. Qiao (2010), Wave-turbulence interaction and its induced mixing in the upper ocean, *J. Geophys. Res.*, *115*, C04026, doi:10.1029/2009JC005853.

Huang, C., F. Qiao, and Z. Song (2008), The effect of the wave-induced mixing on the upper ocean temperature in a climate model, *Acta Oceanol. Sin.*, *27*(3), 104–111.

Huang, C. J., F. Qiao, Z. Song, and T. Ezer (2011), Improving simulations of the upper ocean by inclusion of surface waves in the Mellor-Yamada turbulence scheme, *J. Geophys. Res.*, *116*, C01007, doi:10.1029/2010JC006320.

Hwang, C., and S.-A. Chen (2000), Circulations and eddies over the South China Sea derived from TOPEX/Poseidon altimetry, *J. Geophys. Res.*, *105*(C10), 23,943–23,965, doi:10.1029/2000JC900092.

Large, W. G., and S. Pond (1981), Open ocean momentum flux measurements in moderate to strong winds, *J. Phys. Oceanogr.*, *11*, 324–336, doi:10.1175/1520-0485(1981)011<0324:OOMFMI>2.0.CO;2.

Nasmyth, P. W. (1970), Oceanic turbulence, Ph.D. dissertation, 109 pp., Univ. of B. C,. Vancouver, Canada.

Osborn, T., D. M. Farmer, S. Vagle, S. A. Thorpe, and M. Cure (1992), Measurements of bubble plumes and turbulence from a submarine, *Atmos. Ocean*, *30*(3), 419–440, doi:10.1080/07055900.1992.9649447.

Ozen, B., S. A. Thorpe, U. Lemmin, and T. R. Osborn (2006), Cold-water events and dissipation in the mixed layer of a lake, *J. Phys. Oceanogr.*, *36*, 1928–1939, doi:10.1175/JPO2946.1.

Phillips, O. M. (1961), A note on the turbulence generated by gravity waves, *J. Geophys. Res.*, *66*, 2889–2893, doi:10.1029/JZ066i009p02889.

Prandke, H., and A. Stips (1998), Test measurements with an operational microstructure-turbulence profiler: Detection limit of detection rates, *Aquat. Sci.*, *60*, 191–209, doi:10.1007/s000270050036.

Qiao, F., Y. Yuan, Y. Yang, Q. Zheng, C. Xia, and J. Ma (2004), Wave-induced mixing in the upper ocean: Distribution and application in a global ocean circulation model, *Geophys. Res. Lett.*, *31*, L11303, doi:10.1029/2004GL019824.

Qiao, F., Y. Yuan, T. Ezer, C. Xia, Y. Yang, X. Lü, and Z. Song (2010), A three-dimensional surface wave-ocean circulation coupled model and its initial testing, *Ocean Dyn.*, *60*(5), 1339–1355, doi:10.1007/s10236-010-0326-y.

Rapp, R. J., and W. K. Melville (1990), Laboratory measurements of deep-water breaking waves, *Philos. Trans. R. Soc. London, Ser. A*, *331*, 735–800, doi:10.1098/rsta.1990.0098.

Shay, T. J., and M. C. Gregg (1986), Convectively driven turbulence mixing in the upper ocean, *J. Phys. Oceanogr.*, *16*, 1777–1798, doi:10.1175/1520-0485(1986)016<1777:CDTMIT>2.0.CO;2.

Shu, Q., F. Qiao, Z. Song, C. Xia, and Y. Yang (2011), Improvement of MOM4 by including surface wave-induced vertical mixing, *Ocean Modell.*, *40*, 42–51, doi:10.1016/j.ocemod.2011.07.005.

Simpson, J. H., W. R. Crawford, T. P. Rippeth, A. R. Campbell, and J. S. Cheok (1996), The vertical structure of turbulent dissipation in shelf seas, *J. Phys. Oceanogr.*, *26*, 1579–1590, doi:10.1175/1520-0485(1996)026<1579:TVSOTD>2.0.CO;2.

Soloviev, A., and R. Lukas (2003), Observation of wave-enhanced turbulence in the near-surface layer of the ocean during TOGA COARE, *Deep Sea Res., Part I*, *50*, 371–395, doi:10.1016/S0967-0637(03)00004-9.

Song, Z., F. Qiao, and C. Wang (2011), The correctness to the spuriously simulated semi-annual cycle of the sea surface temperature in the equatorial eastern Pacific, *Sci. China Earth Sci.*, *54*(3), 438–444, doi:10.1007/s11430-011-4176-3.

Stips, A. (2005), Dissipation measurement: Theory, in *Marine Turbulence: Theories, Observations, and Models*, edited by H. Z. Baumert, J. Simpson, and J. Sündermann, pp. 115–126, Cambridge Univ. Press, Cambridge, U. K.

Stips, A., and H. Prandke (2000), Recommended algorithm for dissipation rate calculation within PROVESS, *Tech. Rep. 1.00.116*, 17 pp., Jt. Res. Cent., Eur. Comm., Ispra, Italy.

Thais, L., and J. Magnaudet (1996), Turbulent structure beneath surface gravity waves sheared by the wind, *J. Fluid Mech.*, *328*, 313–344, doi:10.1017/S0022112096008749.

Veron, F., W. K. Melville, and L. Lenain (2009), Measurements of ocean surface turbulence and wave-turbulence interactions, *J. Phys. Oceanogr.*, *39*, 2310–2323, doi:10.1175/2009JPO4019.1.

Wang, Y., F. Qiao, G. Fang, and Z. Wei (2010), Application of wave-induced vertical mixing to the K profile parameterization scheme, *J. Geophys. Res.*, *115*, C09014, doi:10.1029/2009JC005856.

Wen, S. C., and Z. W. Yu (1984), *Theory of Ocean Wave and its Computational Method* (in Chinese), 662 pp., Sci. Press, Beijing.

Wolk, F., H. Yamazaki, L. Seuront, and R. G. Lueck (2002), A new free-fall profiler for measuring biophysical microstructure, *J. Atmos. Oceanic Technol.*, *19*, 780–793, doi:10.1175/1520-0426(2002)019<0780:ANFFPF>2.0.CO;2.

Wüest, A., G. Piepke, and D. C. Van Senden (2000), Turbulence kinetic energy balance as a tool for estimating vertical diffusivity in wind-forced stratified waters, *Limnol. Oceanogr.*, *45*(6), 1388–1400, doi:10.4319/lo.2000.45.6.1388.

Wyrtki, K. (1961), Physical oceanography of the southeast Asian waters, *NAGA Rep. 2*, 195 pp., Univ. of Calif., San Diego, La Jolla.